Selenide-Based Electrocatalysts and Scaffolds for Water Oxidation Applications

*Chuan Xia, Qiu Jiang, Chao Zhao, Mohamed N. Hedhili, and Husam N. Alshareef**

Climate change and the expected shortage of fossil fuels have made it essential that renewable energies such as solar and wind are developed.[1] Electrochemical water splitting ($2H_2O \rightarrow 2H_2 + O_2$) provides a promising option to convert solar energy into chemical fuels, namely hydrogen and oxygen.[2,3] Yet, the realization of efficient water oxidation reactions is greatly hindered by the bottleneck oxygen evolution reaction (OER).[4] This is because OER proceeds through a multistep proton-coupled electron transfer process that is kinetically sluggish.[5,6] A critical requirement for enabling the OER reaction to proceed efficiently is the development of an appropriate electrocatalyst. While the state-of-the-art precious metal RuO_2 or IrO_2 based catalysts are well developed and widely used, a substantial overpotential (η) is still required to initiate the OER.[2] Over the last few decades, extensive efforts have been devoted to designing and synthesizing efficient, durable, and low-cost alternatives based on earth-abundant 3d metals. In particular, currently, cobalt-based OER catalysts have already attracted considerable attention, sparked by its intrinsic corrosion stability in alkali electrolyte, earth-abundant nature, and rich variable valence states. For instance, Hynn et al. reported that a nanostructured $Co(PO_3)_2$ powder catalyst can provide a catalytic onset overpotential of ≈310 mV versus reversible hydrogen electrode (RHE) and a per-metal turnover frequency of 0.10–0.21 s^{-1} at η = 440 mV, whose saturation behavior was observed at a mass loading of >0.6 mg cm^{-2}.[7] Zou et al. showed that Zn–Co layered double hydroxide powder was a much more efficient and durable electrocatalyst in alkaline medium compared with monometallic Co–OH, while the zinc dopant demonstrated as OER inactive site.[8] Furthermore, Li et al. showed that nanostructured nickel substituted cobaltite spinel ($Ni_xCo_{3-x}O_4$) could deliver better OER performance compared to pristine Co_3O_4.[9] Up to now, the efficiency of water oxidation is not satisfactory, and we believe that there is still room to optimize the performance of nanostructured Co-based catalysts for the following reasons: (1) For most material synthesis techniques, a binder and conductive agent are usually required; however, inclusion of the binder and/or conductive agent has been demonstrated to significantly increase the "dead volume" thereby reducing the active material catalytic performance;[10,11] (2) many of the highly active Co-based catalysts including hydroxides, oxides, and chalcogenides are seriously poor conductors; (3) the powder catalyst reaches its saturated performance at a very low geometrical mass loading, thereby resulting in a relatively low catalytic current density and efficiency;[7] (4) recent studies have shown that integrated hybrid catalysts comprising several components can offer a strongly enhanced OER catalytic performance.[12]

To circumvent the above-mentioned disadvantages, several solutions are possible. For example, one could utilize 3D charge conducting nanostructures to scaffold the nonconductive OER active materials and to serve as a self-standing current collector itself, which minimizes the equivalent series resistance (ESR) of such an electrode. In contrast to their bulk and solid counterparts, 3D nanostructures can significantly facilitate bubble convection away from the electrode surface, particularly at high current densities. Such behavior prevents the O_2 bubbles from accumulating and damaging the catalyst, resulting in improved cyclability.[13] Although carbonaceous materials (CNT, graphene) and metals (Au, Ni) have been investigated as backbone materials for a hybrid catalyst, the limited OER activity (in the case of carbonaceous materials) or scarcity/cost (in the case of noble metals) make them impractical choices.[6,10,14] $CoSe_2$ has recently been identified as a promising catalyst for water splitting due to its intrinsic metallicity.[15]

In this study we have investigated the potential of another intrinsically metallic material, $Co_{0.85}Se$, in pure and Ni-doped forms, to be used as OER catalyst. The pristine and Ni-doped $Co_{0.85}Se$ attracted our attention for two reasons. First, the metallic nature of $Co_{0.85}Se$, which is in sharp contrast to the semiconducting nature of other cobalt selenides such as CoSe[16] and Co_9Se_8,[17] made it a potentially useful compound either as electroactive material, or as support material to nonconductive OER compounds. Second, the nickel doping in these cobalt-based materials resulted in nonstoichiometric compositions with unchanged matrix properties, leading to higher electrical conductivity.[18] Moreover, the Ni-doped compositions were found to exhibit higher defect concentrations (dislocation, twin boundary, and stepped surface) which serve as active sites for the catalysis.[19] Therefore, we expected that nanostructured Ni-doped cobalt selenides $(Ni, Co)_{0.85}Se$, with their outstanding conductivity, corrosion resistance, and promising OER activity, could perform well as advanced OER catalysts or to serve as excellent backbone materials for docking insulating OER active materials in hybrid catalysts.

Herein, we report a facile approach to synthesize metallic $Co_{0.85}Se$ and $(Ni, Co)_{0.85}Se$ nanotube arrays on a carbon fabric collector (CFC). The $(Ni, Co)_{0.85}Se$ nanoarrays exhibited higher OER catalytic activity and better reusability than the undoped $Co_{0.85}Se$. Furthermore, the $(Ni, Co)_{0.85}Se$ nanoarrays performed better in alkaline medium than the industrial RuO_2 and IrO_2

C. Xia, Q. Jiang, Dr. C. Zhao, Dr. M. N. Hedhili, Prof. H. N. Alshareef
Materials Science and Engineering
King Abdullah University of Science and Technology (KAUST)
Thuwal 23955-6900, Saudi Arabia
E-mail: husam.alshareef@kaust.edu.sa

DOI: 10.1002/adma.201503906

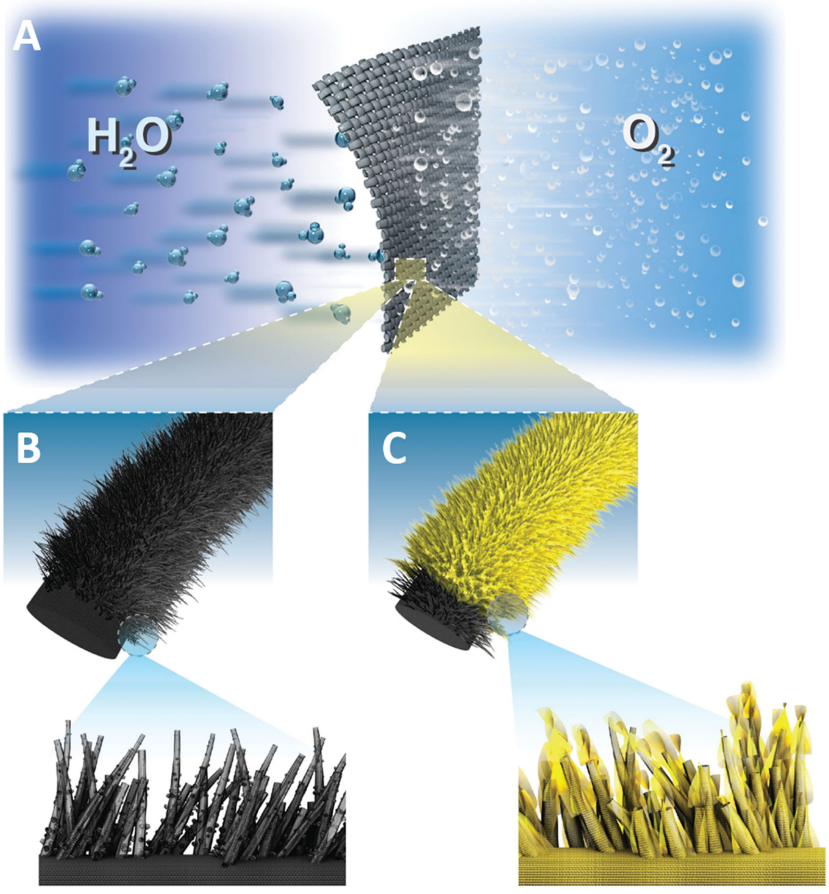

Figure 1. Schematic illustration of the design of A,B) porous nickel cobalt selenide electrocatalyst on carbon cloth and A,C) coaxial hybrid catalyst of (Ni, Co)$_{0.85}$Se@hydroxides.

catalyst, and exhibited superior properties compared to previously reported high-performance Co-based OER catalysts. We show that this remarkable performance enhancement can be attributed to the (1) unique structure and chemical composition and (2) abnormally high concentration of active defect sites in the (Ni, Co)$_{0.85}$Se material system. The fundamental reasons for this remarkable performance will be discussed in detail in the manuscript. We believe that the present work provides a valuable route to achieve an inexpensive and efficient OER electrocatalyst or hybrid catalyst (e.g., in combination with insulating layered double hydroxides).

Morphology- and phase-controllable (Ni, Co)$_{0.85}$Se nanotube arrays were successfully synthesized directly on CFC substrate by a simple hydrothermal process (**Figure 1**A, B). Briefly, the self-sacrificial template of Ni–Co-precursor nanoarrays were fabricated using a hydrothermal method. Afterwards, the Ni–Co precursors were chemically converted in situ into (Ni, Co)$_{0.85}$Se by 1 M fresh NaHSe selenization, resulting in a uniform distribution of Ni, Co, and Se (Note 6, Supporting Information). The electrode fabrication method is described in the experimental section in detail. The CFC was selected as a convenient, flexible, low-cost, chemically inert, highly conductive support that has negligible OER activity. The direct growth of cobalt selenides on CFC substrates gives a convenient, binder-free electrode preparation technique which offers lower contact resistance between the catalyst and substrate, hence minimizing the ohmic losses in the system.[13] X-ray diffraction (XRD) pattern (**Figure 2**A) and inductively coupled plasma optical emission spectroscopy support the formation of hexagonal pure Ni-doped $Co_{0.85}Se$ (JCPDS 52-1008) with a chemical composition of $Ni_{13.8}Co_{32.5}Se_{53.7}$, which is very close to standard (Ni, Co)$_{0.85}$Se. The electrical transport properties of the synthetic selenides were evaluated experimentally from the temperature dependence of resistivity (see the Supporting Information for details). As shown in Figure 2B, the resistivity of the selenides increases linearly with temperature from of 2 to 300 K, indicating their metallic nature. Moreover, the data in Figure 2B clearly shows that the electrical conductivity of (Ni, Co)$_{0.85}$Se is about two times higher than that of pure $Co_{0.85}Se$ at room temperature. Such an excellent conductivity (1.67×10^6 S m^{-1} compared with 9.1×10^6 S m^{-1} for Pt) can facilitate the charge transfer process and minimize the IR losses in the electrode, which is a highly desired feature for high-performance OER catalysts.[20] Importantly, these features of (Ni, Co)$_{0.85}$Se exhibit clear advantages over several material systems such as layered transition metal dichalcogenides and layered double hydroxide, which tend to be less conductive and more costly to produce.[13] The typical scanning electron microscopy (SEM) and transmission electron microscopy (TEM) images show that (Ni,Co)$_{0.85}$Se morphology consists of closely packed and vertically aligned nanotube arrays on CFC, with a diameter and thickness of about 60 nm and 4 μm, respectively (Figure 2C,D and Figure S1, Supporting Information). Similar morphology is obtained for undoped $Co_{0.85}Se$. It is clear that the surface of (Ni, Co)$_{0.85}$Se nanotube is very rough and highly porous, and is composed of numerous nanocrystals in the range of 5–15 nm. The considerable nanocrystal boundaries and mesopores can enhance the specific surface area and contribute to fast mass transport and oxygen diffusion as well.[21]

We have evaluated the OER catalytic performance of selenides directly grown CFC by using them as working electrode without any further treatment. All electrochemical tests were performed in O_2-saturated 1.0 M KOH solution. The catalysts were electrochemically preconditioned to reach a stable state (see the Experimental Section for details). Then, the water oxidation activity was measured by linear sweep voltammetry (LSV). **Figure 3**A shows the IR-corrected (see the Supporting Information for details) LSV curves for representative selenides samples at a low scan rate of 0.5 mV s^{-1}, along with that of a pristine CFC as control. The CFC substrate clearly demonstrates no measurable contribution to the measured signal. While the (Ni, Co)$_{0.85}$Se and $Co_{0.85}Se$ both showed a high-performance toward OER, they exhibited separated oxidation features from the water oxidation. As shown in Figure 3A and

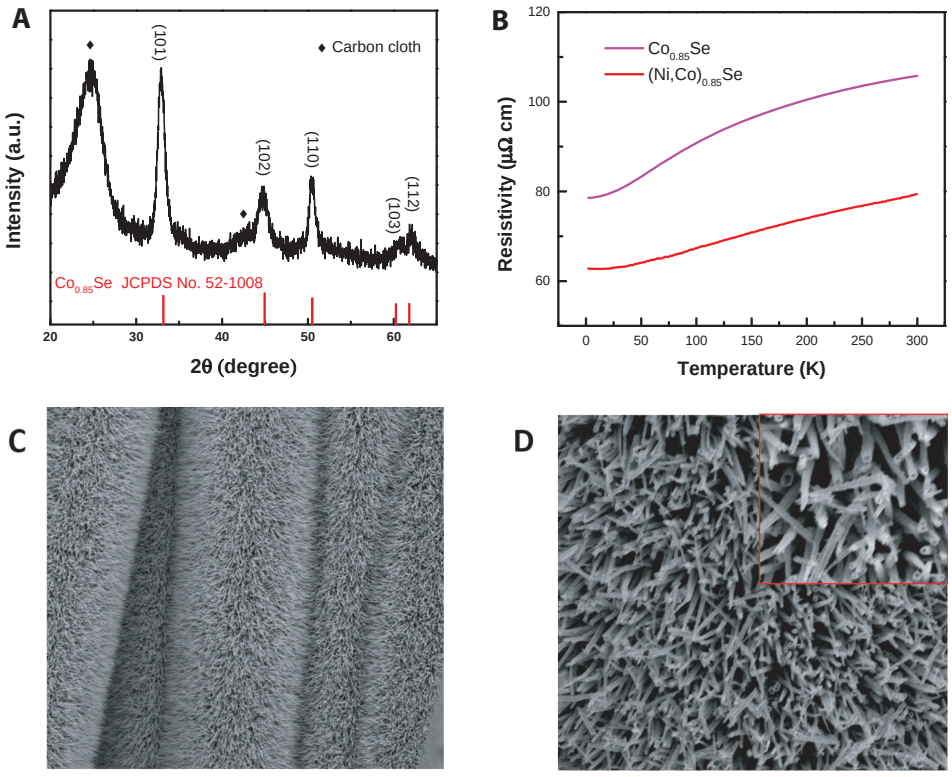

Figure 2. Structural characterization of as-obtained (Ni, $Co)_{0.85}Se$. A) The representative XRD pattern for as-prepared (Ni, $Co)_{0.85}Se$ nanotube arrays on CFC. B) Temperature dependence of resistivity of the (Ni, $Co)_{0.85}Se$ and $Co_{0.85}Se$ pellet compressed from synthetic selenide nanopowders. C,D) The typical SEM images for as-prepared (Ni, $Co)_{0.85}Se$ nanotube arrays on CFC.

Figure S2 (Supporting Information), clear oxidation peaks are observed prior to the onset of oxygen evolution process. $Co_{0.85}Se$ showed two distinctive peaks at 1.303 and 1.381 V versus RHE, which could be assigned to the transformation of Co^{II} to Co^{III} and Co^{III} to Co^{IV}, respectively.[22] Upon Ni doping, the anodic peak of (Ni, $Co)_{0.85}Se$ was broadened and centered at 1.31 V versus RHE with higher intensity. This contribution is due to the oxidation of $Ni^{II}/Ni^{III}/Ni^{IV}$, which proceeds at more negative potential than Co^{III} to Co^{IV} oxidation.[9] In fact, the increase in the area of the anodic peak prior to water oxidation suggests the Ni-doping process also made more active sites accessible. In addition, from the electrochemical impedance spectroscopy, it is obvious that the (Ni, $Co)_{0.85}Se$ exhibited a lower ESR (≈2.2 Ω) and charge transfer resistance (R_{ct}) (≈0.24 Ω) compared with undoped $Co_{0.85}Se$, demonstrating more favorable charge transport kinetics. The exceptional resistance is ascribed to the unique active material/CFC electrode design, and to the incorporation of Ni in the hexagonal $Co_{0.85}Se$ lattice.[23] It is worthwhile to mention that such a low ESR can endow an efficient pathway for electron transportation at the electrolyte/electrode interface and the electrode bulk as well, which minimizes IR losses. In order to further check the accessibility of electrolyte to our electrode active material, the contact angles of all studied samples were examined. Amazingly, while the CFC substrate shows a superhydrophobic nature with a contact angle of 161°, our as-prepared selenides catalysts, with or without Ni doping, both show superhydrophilic behavior (Figure S3 and supplementary videos, Supporting Information). The superhydrophilic nature of selenide-covered CFC means the aqueous solution easily spreads on the entire surface (external and internal) of the selenide-covered CFC, hence boosting the electrolyte ion trapping and access to the active sites. The superhydrophilic behavior suggests that our selenide-coated CFC was surface-hydroxylated to some extent, either due to surface oxyhydroxide or the substitution of oxygen atoms at the surface of hydroxyl groups.[10,24]

As commonly adopted in the electrocatalysis community,[2,9,21,25] three parameters were calculated to quantify the improvement of OER activity: the overpotential at a current density (J) of 10 mA cm^{-2}, the current density at an overpotential (η) of 300 mV, and the Tafel slope. The current density of 10 mA cm^{-2} was suggested by Hu[2] and Yu,[26] considering the upper end of a realistic solar device with 12% solar to hydrogen efficiency. Figure 3A clearly shows that the catalytic currents were significantly shifted to lower potential upon Ni doping. Specifically, at J = 10 mA cm^{-2}, (Ni, $Co)_{0.85}Se$ exhibits an overpotential of 255 mV versus RHE. In comparison, pristine $Co_{0.85}Se$ exhibits an overpotential of 324 mV to achieve significant O_2 evolution (J = 10 mA cm^{-2}). The higher activity of (Ni, $Co)_{0.85}Se$ was also evident from the larger current density compared with other control electrodes. At a fixed overpotential of 300 mV versus RHE, (Ni, $Co)_{0.85}Se$ delivered a current density of 36.4 mA cm^{-2} which is ≈7 times higher than pure $Co_{0.85}Se$ (5.3 mA cm^{-2}). If the applied potential increases to 1.59 V versus RHE, the (Ni, $Co)_{0.85}Se$ shows a high current density of 122 mA cm^{-2}, while the pure $Co_{0.85}Se$ only shows a modest

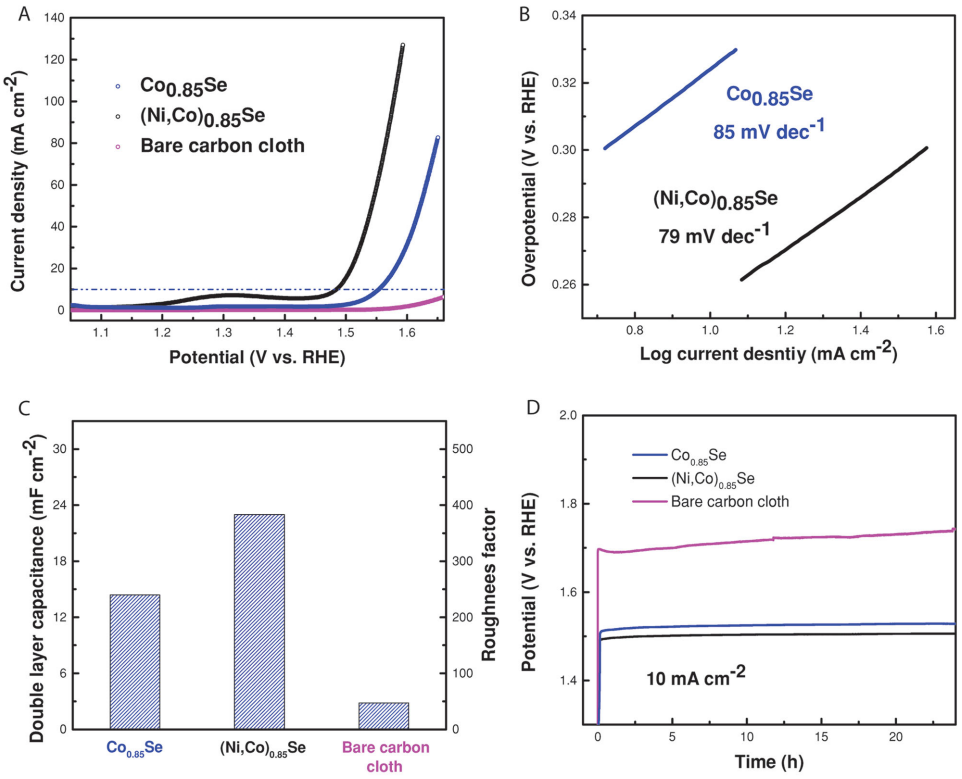

Figure 3. OER activities and stabilities of selenide materials. Electrochemical properties of different selenides deposited directly on carbon fiber (CFC). A) IR-corrected LSV curves of $Co_{0.85}Se$, (Ni, Co)$_{0.85}$Se, and CFC substrate and B) the corresponding Tafel plots. C) Comparison of the double-layer capacitance (ECSA) and corresponding R_f of each electrode. D) Long-term stability measurements at $J = 10$ mA cm^{-2} for all studied samples.

OER activity (25 mA cm^{-2}). The improved OER performance of (Ni, Co)$_{0.85}$Se was further reflected in their lower Tafel slope (Figure 3B). The Tafel slope of (Ni, Co)$_{0.85}$Se and $Co_{0.85}Se$ are 79 and 85 mV dec^{-1}, respectively. This suggests the reaction kinetics for Ni-doped samples are more favorable than undoped $Co_{0.85}Se$. Besides, the lower Tafel slopes of (Ni, Co)$_{0.85}$Se can afford an even higher enhancement in OER activity at $\eta > 300$ mV, because its current density increased more rapidly with an increase of overpotential.[2] Electrochemical active surface area (ECSA) and corresponding roughness factor (R_f) are often primarily responsible for enhanced catalytic activity in nanostructured catalysts. In an attempt to understand the significant difference in performance between $Co_{0.85}Se$ and (Ni, Co)$_{0.85}$Se, the ECSA and corresponding R_f were estimated from the electrochemical double-layer capacitance (C_{dl}) (see the Supporting Information for details). Figure 3C shows the effective ECSA of the solid–liquid interface of each electrode. The C_{dl} of (Ni, Co)$_{0.85}$Se was 22.99 mF cm^{-2}, whereas that of $Co_{0.85}Se$ was 14.405 mF cm^{-2}. This comparison reveals that (Ni, Co)$_{0.85}$Se reached to 60% increase of the ECSA and R_f after Ni doping. It is likely that this enhancement in ECSA primarily accounts for the differences in performance, indicating that the number of active sites for water oxidation was increased significantly after Ni doping, shedding light on the mechanism of improved OER performance. It is worth mentioning that such a high ECSA and R_f are superior to previously reported 3D nanostructured electrocatalysts.[2,9,10,13,22,25] Another major concern is the durability of the electrode for water oxidation. As shown in Figure 3D, the stabilities of as-obtained catalysts were tested at a constant current density of 10 mA cm^{-2} for 24 h. Noticeably, over the duration of the 24 h electrolysis, the overpotential of (Ni, Co)$_{0.85}$Se electrodes remained nearly constant, demonstrating excellent stability. Initially, the (Ni, Co)$_{0.85}$Se requires an overpotential of 255 mV versus RHE to drive an efficient water oxidation ($J = 10$ mA cm^{-2}). After long-term stability measurements, an overpotential of 276 mV versus RHE was needed to maintain the same current density of 10 mA cm^{-2}, increasing by only 21 mV versus RHE. Such stability is also believed to correlate with the vertically aligned nature of the selenide nanostructures. Song and co-workers proposed the following explanations to address this correlation. At a high current density, the production of O_2 bubbles is vigorous, the nanotubes, to some degree, are superior in facilitating bubble convection away from the electrode surface, hence avoiding any reduction in the ECSA. Such behavior prevents the bubbles from accumulating and damaging the catalysts, as commonly occurs for the solid or bulk materials. In this fashion, vertically aligned nanostructures can enhance the performance and reusability of the catalyst.[13] In fact, the performance of our (Ni, Co)$_{0.85}$Se catalyst is superior to previously reported high-performance Co-based OER catalysts (Table S1, Supporting Information), as well as commercially used RuO_2 and IrO_2 catalysts.

It has been proposed that the different surface characteristics, particularly surface defects, can significantly impact the electrochemical activity of the catalysts.[19] To better understand the origin of the excellent OER activity of (Ni, Co)$_{0.85}$Se, X-ray

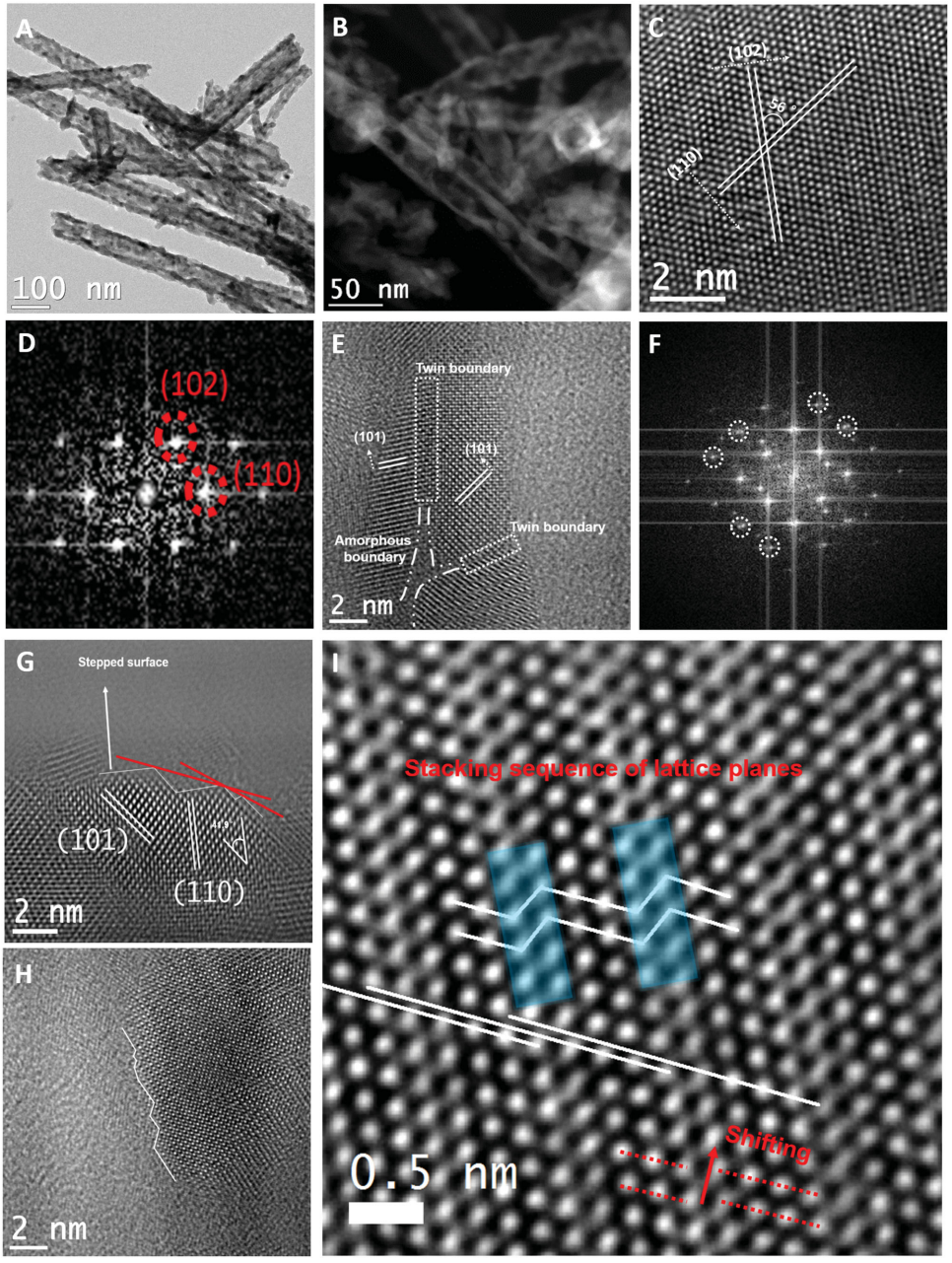

Figure 4. Microstructure characterization of (Ni, $Co)_{0.85}Se$. A,B) The typical TEM and high-angle annular dark-field scanning transmission electron microscopy (HAADF-STEM) images for as-prepared (Ni, $Co)_{0.85}Se$ nanotube arrays on CFC. C–I) The aberration-corrected HRTEM images of as-obtained (Ni, $Co)_{0.85}Se$ nanotubes with the corresponding FFT images, which were obtained at or near the surface.

photoelectron spectroscopy (XPS) and aberration-corrected high-resolution TEM (HRTEM) studies were carried out. As shown in **Figure 4**A,B, the rough nature of the surface of highly porous selenide nanotubes is confirmed. Furthermore, Figure 4C reveals well-defined lattice fringes with spacing of ≈0.2 and ≈0.18 nm, which could be readily indexed to (102) and (110) planes of $Co_{0.85}Se$, in agreement with the conclusion from the corresponding fast Fourier transformation (FFT) (Figure 4D). Previous investigations on catalyst systems have suggested that surface defects and lattice strain play a crucial role in the catalyst material performance.[19,27,28] Hence, we performed a detailed structural study of the surface of $Co_{0.85}Se$ and (Ni, $Co)_{0.85}Se$ nanotubes using aberration-corrected HRTEM. The analysis of several samples consistently showed that (Ni, $Co)_{0.85}Se$ had a significantly higher defect concentration (of various types) than $Co_{0.85}Se$. These defects include planar extended defects, stacking faults, and twin boundaries, which run across the entire nanocrystal surfaces. For example, Figure 4E shows a typical pattern of planar bulk defects (twin boundaries) whose existence can be corroborated from the corresponding FFT diffraction pattern shown in Figure 4F (The extra diffraction spots (see circles) are clearly visible).

ADVANCED MATERIALS
www.advmat.de

www.MaterialsViews.com

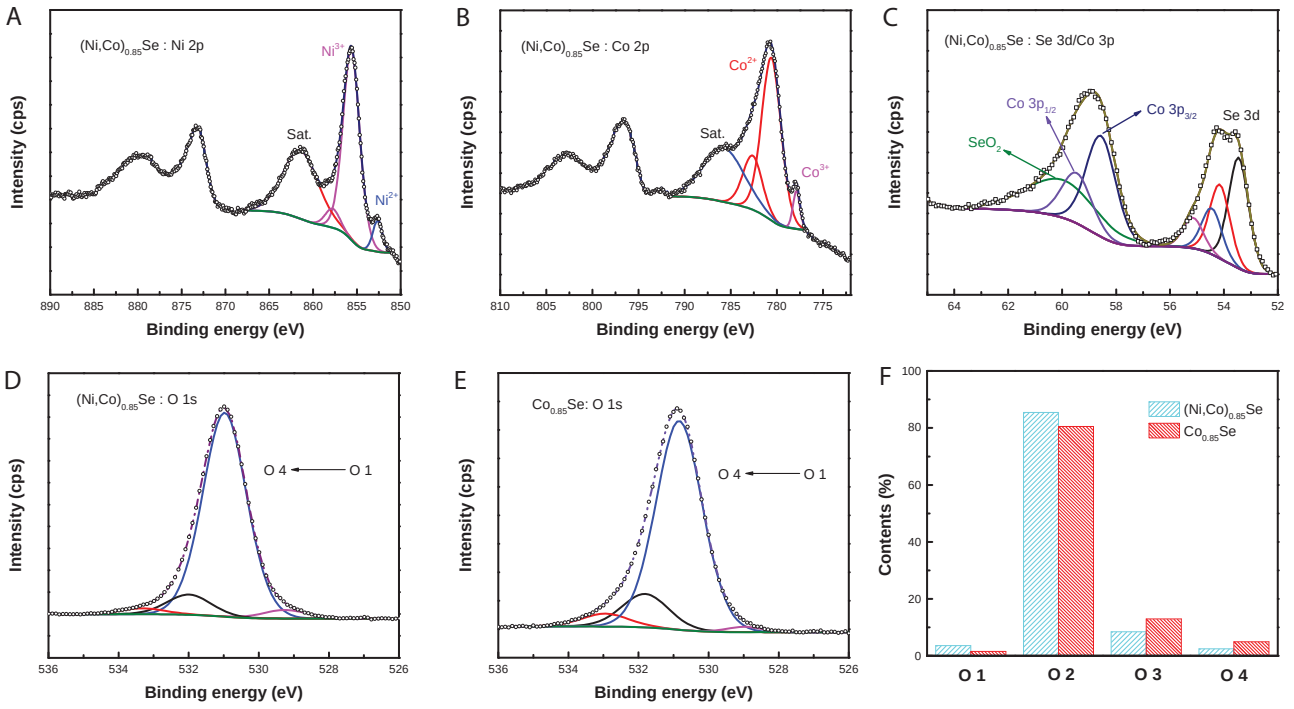

Figure 5. Detailed XPS analysis of as-prepared selenides. High resolution XPS spectra for A) Ni 2p, B) Co 2p, and C) Se 3d/Co 3p and peak fitting analysis of as-prepared (Ni, Co)$_{0.85}$Se. The O 1s region of XPS spectra of as-obtained D) (Ni, Co)$_{0.85}$Se and E) Co$_{0.85}$Se. F) Summary of the relative content from the O^{I} to O^{IV} subbands in (D) and (E).

Figure 4G,H shows another type of defect, namely, the stepped surface or the stacking fault-created step facets at the surface of (Ni, Co)$_{0.85}$Se, leading to the exposure of high-index facets (red line in Figure 4G). While high-index facets at the surface of crystals are generally expected to be unstable, due to their high surface energy, they can be strongly stabilized in the presence of a significant number of other surface atomic steps.[28,29] It has also been suggested that the stepped surfaces could also be stabilized by a series of well-defined bulk defects.[19] In addition, it has been demonstrated that the high density of atomic steps at the surface could promote molecular adsorption due to reduced chemical reaction potential barriers, which is believed to give rise to better OER catalytic behavior.[30] Figure 4I and Figure S4 (Supporting Information) further demonstrate that twins could create distinctive surface ensembles even if the (Ni, Co)$_{0.85}$Se surface of a large particle appears essentially flat. By carefully inspecting the stacking sequence of lattice planes, we notice that a series of atoms were misplaced out of their regular position (see straight white line in Figure 4I). In contrast to (Ni, Co)$_{0.85}$Se, the defects in Co$_{0.85}$Se are observed in significantly lower concentrations (Figure S5, Supporting Information). The higher defects density in (Ni, Co)$_{0.85}$Se is presumably induced by the Ni-doping process, a result which can be attributed to difference in physical and chemical properties between nickel and cobalt ions, a phenomenon that has been widely observed.[31] To sum up, a significant concentration of defects has been observed in (Ni, Co)$_{0.85}$Se catalyst, but not Co$_{0.85}$Se. These defects are high-energy sites that serve as active sites in the water oxidation process, making the defect-rich metallic (Ni, Co)$_{0.85}$Se an efficient OER catalyst.

According to the XPS analysis, the survey spectra of (Ni, Co)$_{0.85}$Se (Figure S6, Supporting Information) demonstrate the appearance of Ni, Co, and Se peaks, showing that Ni has been successfully introduced into the Co$_{0.85}$Se lattice. The peak fitting analysis of Ni 2p (**Figure 5**A) shows that the chemical species of Ni can be identified as Ni^{2+} (852.65 eV) and Ni^{3+} (855.62 eV), with binding energies that are close to those reported for nickel chalcogenides (NiSe,[32] $NiSe_2$,[33] and $NiCo_2S_4$.[34] Besides, another peak of Ni^{3+}centered at 857.78 eV might be evidence for γ-NiOOH formation at the surface.[35,36] On the basis of in situ X-ray absorption near-edge structure spectroscopy studies, Bediako et al. pointed out that the γ-NiOOH phase is crucial to achieving high OER activity among Ni-based catalysts. This also implies that surface exposed Ni and Co are both highly active sites in our (Ni, Co)$_{0.85}$Se, resulting in a higher activity than undoped Co$_{0.85}$Se. Similarly, in the Co 2p spectra of (Ni, Co)$_{0.85}$Se (Figure 5B), the binding energy at 778.88 eV can be ascribed to Co^{3+}, while 780.59 and 782.64 eV can be ascribed to Co^{2+}, suggesting the coexistence of cobalt selenides, oxides, or hydroxides near the surface.[21,25,34] Furthermore, and interestingly, detailed analysis of Se 3d high-resolution XPS spectra (Figure 5C) shows that there are two different kinds of metal–selenium bonds (Se $3d_{5/2}$ at 53.6 and 54.2 eV, respectively) present in the (Ni, Co)$_{0.85}$Se crystal. We believe that this observation strongly supports the successful incorporation of Ni into Co$_{0.85}$Se lattice to form two kinds of metal–Se bonds (Ni–Se and Co–Se). The binding energy at 60 eV is likely related to SeO_2.[37] That means that the surface of (Ni, Co)$_{0.85}$Se was contaminated, to some degree, by undesired SeO_2, which was further demonstrated by the TEM and energy-dispersive

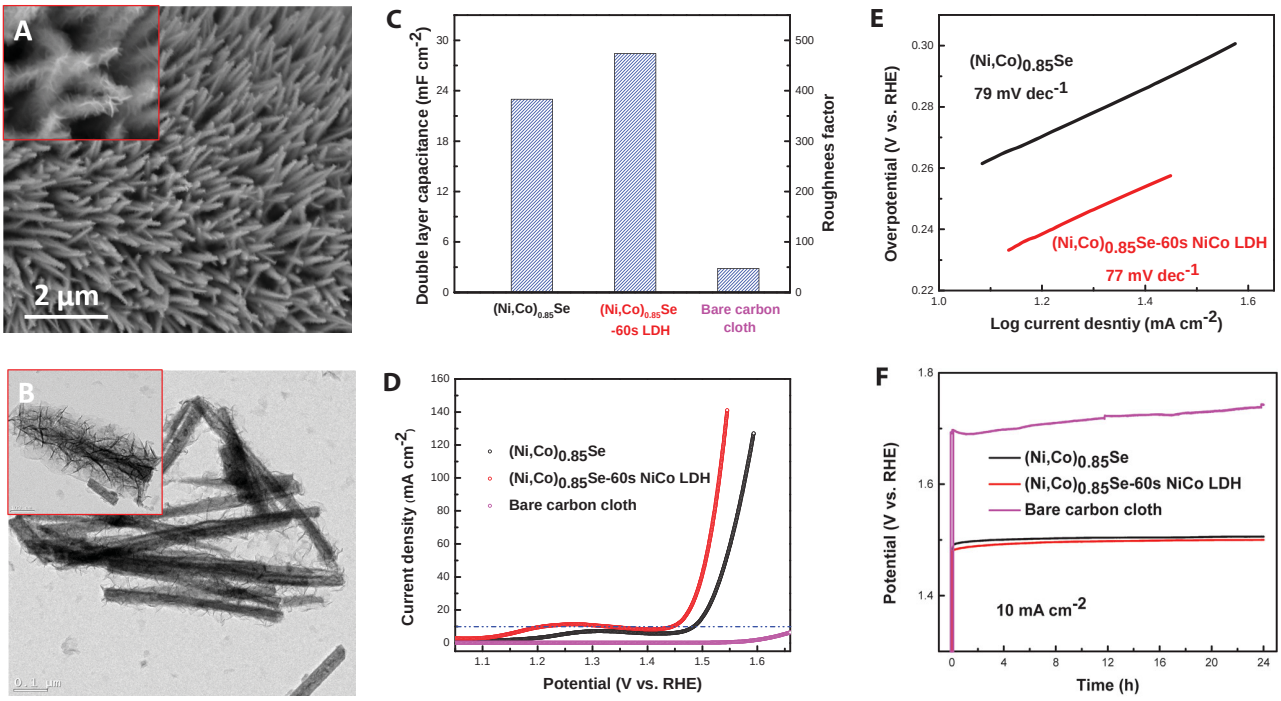

Figure 6. TEM images and electrochemical behavior of coaxial hybrid catalyst. A,B) The typical SEM and TEM images of fresh (Ni, Co)$_{0.85}$Se@NiCo-LDH coaxial nanotubes. C) Comparison of the ECSA (C_{dl}) and corresponding R_f of all studied electrode. D) Polarization curves of (Ni, Co)$_{0.85}$Se and (Ni, Co)$_{0.85}$Se@NiCo-LDH with corresponding E) Tafel curves. F) Chronopotentiometric measurements at J = 10 mA cm^{-2} for as-prepared selenides, along with that of CFC as control.

spectroscopy analysis (Figure S7, Supporting Information). However, these amorphous SeO_2 surface layers are removed during the electrochemical preconditioning process we typically conduct before LSV measurements in 1 M KOH. Unlike (Ni, Co)$_{0.85}$Se, we only observe one kind of typical metal–Se bond, namely Co–Se bond, in the Se 3d XPS spectra of Co$_{0.85}$Se (Figure S8, Supporting Information). To gain more insights into the OER activity, the surface oxygen state was studied because they always function as active sites in the water oxidation reaction.[21,38] Figure 5D,E reveals that the O 1s spectra could be fitted into four contributions coming from both (Ni, Co)$_{0.85}$Se and Co$_{0.85}$Se, henceforth referred to as O^{I} (low binding energy) to O^{IV} (high binding energy). The O^{I} contribution (529.0–529.2 eV) can be attributed to the metal–oxygen bonds, probably Ni/Co–O(OH). The second contribution (O^{II}) around 530.8–530.9 eV is likely associated with oxygen in –OH groups, indicating the surfaces of our selenides were hydroxylated.[36] In agreement with the Se 3d spectra, the O^{III} (531.8–531.9 eV) can be attributed to the surface-absorbed SeO_2.[39] The peak located at 533.1–533.3 eV (O^{IV}) is believed to provide evidence for the presence physi-sorbed- and chemi-sorbed water at or near the surface. The relative content of the four contributions in O 1s is summarized in Figure 5F. Of note, (Ni, Co)$_{0.85}$Se possess a higher content of surface functional group (–OH) compared to pure Co$_{0.85}$Se (85.42% vs 80.54%), which may result in more accessible active sites in the former. On the other hand, the better hydroxylated surface can be more ion-permeable and favorable to water oxidation in these superhydrophilic compounds.

To further evaluate the potential of (Ni, Co)$_{0.85}$Se nanotube arrays for electrocatalysis applications, we fabricated a hybrid catalyst electrode directly on CFC (Figure 2A,C) using a combination of metallic (Ni, Co)$_{0.85}$Se and an insulating layered double hydroxide compound (NiCo-LDH). NiCo-LDH was selected because it has been reported to be an excellent insulating OER active material.[2,25] As shown in **Figure 6**A,B and Figure S9 (Supporting Information), the electrodeposited NiCo-LDH had a unique morphology consisting of curved mesoporous nanosheets with few layer (4–8 atomic layers) thickness, which is reminiscent of chemically exfoliated transition metal dichalcogenides and layered double hydroxides. This unique structure is likely to achieve a better OER performance due to the following reasons: (1) the accessibility of electrolyte ions into metallic (Ni, Co)$_{0.85}$Se will not be blocked by the ultrathin mesoporous NiCo-LDH; (2) the coaxial catalyst provides a higher ECSA and R_f (Figure 6C); (3) the surface decorated LDHs (M(OH)$_2$ or MOOH) are more ion-permeable; (4) the electron transportation of insulating NiCo-LDH could be strongly boosted using metallic (Ni, Co)$_{0.85}$Se. In fact, as a result of this unique structure, we observed a huge jump in the catalytic performance of (Ni, Co)$_{0.85}$Se@NiCo-LDH as evidenced by the OER results. Figure 6D shows that the measured over overpotentials (at J = 10 mA cm^{-2}) are 216 mV for (Ni, Co)$_{0.85}$Se@NiCo-LDH and 255 mV for (Ni, Co)$_{0.85}$Se. Comparing the current densities at overpotential of 300 mV, an ≈2.7-folds enhancement was observed for the hybrid catalyst (97.5 vs 36.4 mA cm^{-2}). This result clearly supports the fact that higher OER activity can be obtained using the hybrid catalyst. Besides, the enhanced kinetics of

(Ni, Co)$_{0.85}$Se@NiCo-LDH, the hybrid catalyst showed a relatively lower Tafel slope of 77 mV dec^{-1} (Figure 6E), compared with that of (Ni, Co)$_{0.85}$Se (79 mV dec^{-1}). Furthermore, the mass activity of (Ni, Co)$_{0.85}$Se and (Ni, Co)$_{0.85}$Se@NiCo-LDH at overpotential of 300 mV was calculated to be 7.28 and 16.25 A g^{-1}, respectively. This estimation agreed with our previous prediction, indicating a jump of the OER capability for the hybrid catalyst. The durability of the hybrid electrode was also investigated and is shown in Figure 6F. After a continuous 24 h electrolysis reaction, only a 24 mV increase in the overpotential required to carry forward an efficient water oxidation (at J = 10 mA cm^{-2}) was observed (from 216 to 240 mV). This result suggests an attractive stability of our hybrid catalyst in alkaline electrolytes.

Based on the results presented in this study, we believe that a unique and advanced OER catalyst has been achieved. Our metallic (Ni, Co)$_{0.85}$Se nanoarrays not only play a role as OER active material, but also serve as an advanced 3D scaffold on which hybrid electrocatalysts can be fabricated. The obvious performance improvement in this study can be explained as follows. First, Ni doping induces an approximately twofolds increase in the conductivity of Co$_{0.85}$Se. Additionally, a higher density of edge defects and larger accessible ECSA are simultaneously obtained by Ni doping. It has widely accepted that materials with more abundant edge sites and higher conductivity can exhibit higher OER activity.[2] In our case, the unique composition and nanostructure of our (Ni, Co)$_{0.85}$Se electrodes lead to the existence of high concentration of surface vacancies and defects, resulting in significant formation and exposure of electrochemical active sites like Co^{4+}. For OER, its activity is significantly influenced by the O atomic adsorption from the electrocatalyst, in which the adsorption energy of the O atom on the catalyst surface plays an essential role. Recent reports pointed out that high oxidation state cations were believed to enhance the electrophilicity of the adsorbed O and thus to facilitate the formation of O–OH (hypothesized as rate-limiting step) via nucleophilic attack, which was also thought to promote the deprotonation of the OOH species, via electron-withdrawing inductive effect, to produce O_2.[26,40] Also, the abundant vacancies which result in the formation of extra dangling bonds were commonly recognized as promising feature to reduce the surface adsorption energy and further improve the overall electrocatalytic performance.[41] Second, the highly mesoporous structure and higher hydroxylation degree of (Ni, Co)$_{0.85}$Se allow faster mass transport and better ion permeation, facilitating the dissociation of water. Third, the unique nanostructures are favorable to maintaining the effective ECSA in the vigorous OER stage. Meanwhile, the direct electrodeposition of ultrathin NiCo-LDH on (Ni, Co)$_{0.85}$Se nanotubes cause a robust integrated electrode, providing a pathway for fast electron and electrolyte transportation. The decorated NiCo-LDH ultrathin nanosheets can further stabilize, to some degree, the (Ni, Co)$_{0.85}$Se nanotube arrays as a protection layer. Moreover, the synergistic effect from the two components is also considered as another important aspect of the hybrid electrode. For instance, Yu and co-workers showed the performance of Mn_3O_4/$CoSe_2$ hybrid catalyst can be improved by the electron donation from Mn_3O_4 to $CoSe_2$, making a more acidic Lewis acid to gain better activation of H_2O (Lewis base) molecules.[26] From another perspective, our binder-free fabrication technique can greatly minimize the ohmic losses, which are very fundamental for practical application.

In general, we show that metallic (Ni, Co)$_{0.85}$Se nanotube arrays on CFC are ideal OER electrocatalysts, competing favorably against previously reported 3d-metal based alternatives. Subsequently, we clearly describe the importance of Ni doping regarding the enhancement of OER performance of Co$_{0.85}$Se. More importantly, we also prove that our as-prepared (Ni, Co)$_{0.85}$Se nanotube arrays are promising 3D scaffolds for other insulating highly active OER materials to make hybrid catalysts. This concept was successfully demonstrated using (Ni, Co)$_{0.85}$Se@NiCo-LDH as a hybrid catalyst. Given their low-cost and ease of fabrication over large areas, our study demonstrates a new approach to achieve promising OER catalysts, particularly a hybrid alternative.

Experimental Section

Experimental details are included in the Supporting Information.

Supporting Information

Supporting Information is available from the Wiley Online Library or from the author.

Acknowledgements

Research reported in this publication was supported by King Abdullah University of Science and Technology (KAUST). The authors wish to thank Dr. Xin He and Dr. Peng Li at KAUST for their help with the AFM analysis.

Received: August 11, 2015
Revised: September 30, 2015
Published online: November 5, 2015

[1] P. Simon, Y. Gogotsi, *Nat. Mater.* **2008**, *7*, 845.
[2] F. Song, X. Hu, *Nat. Commun.* **2014**, *5*, 4477.
[3] Y. Meng, W. Song, H. Huang, Z. Ren, S.-Y. Chen, S. L. Suib, *J. Am. Chem. Soc.* **2014**, *136*, 11452.
[4] a) J. B. Gerken, J. G. McAlpin, J. Y. Chen, M. L. Rigsby, W. H. Casey, R. D. Britt, S. S. Stahl, *J. Am. Chem. Soc.* **2011**, *133*, 14431; b) F. Jiao, H. Frei, *Energy Environ. Sci.* **2010**, *3*, 1018.
[5] M. Gao, W. Sheng, Z. Zhuang, Q. Fang, S. Gu, J. Jiang, Y. Yan, *J. Am. Chem. Soc.* **2014**, *136*, 7077.
[6] M. Gong, Y. Li, H. Wang, Y. Liang, J. Z. Wu, J. Zhou, J. Wang, T. Regier, F. Wei, H. Dai, *J. Am. Chem. Soc.* **2013**, *135*, 8452.
[7] H. S. Ahn, T. D. Tilley, *Adv. Funct. Mater.* **2013**, *23*, 227.
[8] X. Zou, A. Goswami, T. Asefa, *J. Am. Chem. Soc.* **2013**, *135*, 17242.
[9] Y. Li, P. Hasin, Y. Wu, *Adv. Mater.* **2010**, *22*, 1926.
[10] Z. Zhao, H. Wu, H. He, X. Xu, Y. Jin, *Adv. Funct. Mater.* **2014**, *24*, 4698.
[11] W. Liu, C. Lu, X. Wang, K. Liang, B. K. Tay, *J. Mater. Chem. A* **2015**, *3*, 624.
[12] a) G. M. Carroll, D. K. Zhong, D. R. Gamelin, *Energy Environ. Sci.* **2015**, *8*, 577; b) L. Y. S. Lee, K.-Y. Wong, *Organometallics and Related Molecules for Energy Conversion*, Springer, New York **2015**, p. 365.
[13] M. S. Faber, R. Dziedzic, M. A. Lukowski, N. S. Kaiser, Q. Ding, S. Jin, *J. Am. Chem. Soc.* **2014**, *136*, 10053.
[14] S. Chen, S.-Z. Qiao, *ACS Nano* **2013**, *7*, 10190.
[15] a) Y. R. Zheng, M. R. Gao, Q. Gao, H. H. Li, J. Xu, Z. Y. Wu, S. H. Yu, *Small* **2015**, *11*, 182; b) Y. Liu, H. Cheng, M. Lyu, S. Fan, Q. Liu, W. Zhang, Y. Zhi, C. Wang, C. Xiao, S. Wei, *J. Am. Chem. Soc.* **2014**,

136, 15670; c) M.-R. Gao, X. Cao, Q. Gao, Y.-F. Xu, Y.-R. Zheng, J. Jiang, S.-H. Yu, *ACS Nano* **2014**, *8*, 3970; d) D. S. Kong, H. T. Wang, Z. Y. Lu, Y. Cui, *J. Am. Chem. Soc.* **2014**, *136*, 4897.

[16] M. L. Gaur, P. P. Hankare, K. M. Garadkar, I. S. Mulla, V. M. Bhuse, *New J. Chem.* **2014**, *38*, 255.

[17] X. Zhang, J. Zhang, J. Zhao, B. Pan, M. Kong, J. Chen, Y. Xie, *J. Am. Chem. Soc.* **2012**, *134*, 11908.

[18] C. Yuan, H. B. Wu, Y. Xie, X. W. D. Lou, *Angew. Chem. Int. Ed.* **2014**, *53*, 1488.

[19] M. Behrens, F. Studt, I. Kasatkin, S. Kühl, M. Hävecker, F. Abild-Pedersen, S. Zander, F. Girgsdies, P. Kurr, B.-L. Kniep, *Science* **2012**, *336*, 893.

[20] M. A. Lukowski, A. S. Daniel, F. Meng, A. Forticaux, L. Li, S. Jin, *J. Am. Chem. Soc.* **2013**, *135*, 10274.

[21] H. Shi, G. Zhao, *J. Phys. Chem. C* **2014**, *118*, 25939.

[22] X. Liu, Z. Chang, L. Luo, T. Xu, X. Lei, J. Liu, X. Sun, *Chem. Mater.* **2014**, *26*, 1889.

[23] W. King, A. Tseung, *Electrochim. Acta* **1974**, *19*, 485.

[24] C. Yuan, J. Li, L. Hou, X. Zhang, L. Shen, X. W. D. Lou, *Adv. Funct. Mater.* **2012**, *22*, 4592.

[25] H. Liang, F. Meng, M. Cabán-Acevedo, L. Li, A. Forticaux, L. Xiu, Z. Wang, S. Jin, *Nano Lett.* **2015**, *15*, 1421.

[26] M.-R. Gao, Y.-F. Xu, J. Jiang, Y.-R. Zheng, S.-H. Yu, *J. Am. Chem. Soc.* **2012**, *134*, 2930.

[27] a) I. Kasatkin, P. Kurr, B. Kniep, A. Trunschke, R. Schlögl, *Angew. Chem.* **2007**, *119*, 7465; b) M.-T. Nguyen, S. Piccinin, N. Seriani, R. Gebauer, *ACS Catal.* **2014**, *5*, 715; c) M. M. Günter, T. Ressler, B. Bems, C. Büscher, T. Genger, O. Hinrichsen, M. Muhler, R. Schlögl, *Catal. Lett.* **2001**, *71*, 37.

[28] X. Yu, Z. Sun, Z. Yan, B. Xiang, X. Liu, P. Du, *J. Mater. Chem. A* **2014**, *2*, 20823.

[29] J. P. Perdew, J. Chevary, S. Vosko, K. A. Jackson, M. R. Pederson, D. Singh, C. Fiolhais, *Phys. Rev. B* **1992**, *46*, 6671.

[30] G. A. Somorjai, D. Blakely, *Nature* **1975**, *258*, 580.

[31] a) S. B. Ogale, *Adv. Mater.* **2010**, *22*, 3125; b) M. Pashley, K. Haberern, *Phys. Rev. Lett.* **1991**, *67*, 2697; c) Y.-S. Kim, C. Park, *Phys. Rev. Lett.* **2009**, *102*, 086403.

[32] R. Shalvoy, P. Reucroft, *J. Vac. Sci. Technol.* **1979**, *16*, 567.

[33] H. Van der Heide, R. Hemmel, C. Van Bruggen, C. Haas, *J. Solid State Chem.* **1980**, *33*, 17.

[34] W. Chen, C. Xia, H. N. Alshareef, *ACS Nano* **2014**, *8*, 9531.

[35] M. S. Hamdan, Riyanto, M. R. Othman, *Int. J. Electrochem. Sci.* **2013**, *8*, 4747.

[36] M. C. Biesinger, B. P. Payne, A. P. Grosvenor, L. W. Lau, A. R. Gerson, R. S. C. Smart, *Appl. Surf. Sci.* **2011**, *257*, 2717.

[37] U. Weser, G. Sokolowski, W. Pilz, *J. Electron Spectrosc. Relat. Phenom.* **1977**, *10*, 429.

[38] Y. Zhang, G. Zhao, Y. Zhang, X. Huang, *Green Chem.* **2014**, *16*, 3860.

[39] D. Rajamanickam, P. Dhatshanamurthi, M. Shanthi, *Spectrochim. Acta, Part A: Mol. Biomol. Spectrosc.* **2015**, *138*, 489.

[40] B. S. Yeo, A. T. Bell, *J. Am. Chem. Soc.* **2011**, *133*, 5587.

[41] Y. Li, H. Wang, H. Zhang, P. Liu, Y. Wang, W. Fang, H. Yang, Y. Li, H. Zhao, *Chem. Commun.* **2014**, *50*, 5569.